Applicability of Shockley–Read–Hall Theory for Interface States

Bernhard Ruch, Markus Jech, Gregor Pobegen, and Tibor Grasser, *Fellow, IEEE*

***Abstract*— The Shockley–Read–Hall (SRH) model has been successfully used for decades to describe the dynamics of interface states. Interestingly, the SRH model neglects structural relaxation at the defect site, which has a dramatic effect on the dynamics of oxide defects. One may, therefore, wonder why this omission has not led to serious and obvious discrepancies with experimental data. Using *ab initio* approaches to investigate Si dangling bonds, known as P_b centers, within a realistic Si/a-SiO_2 environment together with the more complete nonradiative multiphonon (NMP) theory, we explore why the SRH model provides an excellent approximation for interface traps but not for bulk oxide defects. We will also show that the commonly used Arrhenius correction of the capture cross section can be used to introduce a modified SRH model, which provides a reasonable approximation to the results obtained from a full NMP approach. However, it is shown that this Arrhenius correction may lead to incorrect relaxation energy estimations, especially for bulk oxide defects.**

***Index Terms*— Charge pumping (CP), hot carrier degradation, MOSFET, nonradiative multiphonon (NMP), reliability, silicon, spectroscopic charge pumping (SPCP).**

I. Introduction

THE Shockley–Read–Hall (SRH) theory [1] is one of the most popular models for the transition dynamics between channel carriers and defects [2]–[4]. Unfortunately, it does not consider the structural change of the defects upon changes of its charge state. In order to include this effect, a nonradiative multiphonon (NMP) model [5] can be employed instead. It takes a relaxation energy due to structural reconfigurations of the involved defects into account. This relaxation energy is difficult to measure directly but can be extracted from density functional theory (DFT) calculations. The main issues are credible atomistic Si/SiO_2 models. From three defects identified in [6], the interface defect that shows closest resemblance with a P_b center [7]–[9] is used for further investigations. In order to benchmark the SRH model against the NMP model, experimental spectroscopic charge pumping (SPCP) data are used since this method requires data recorded over a wide temperature range. Thereby, the analysis should be very sensitive to structural relaxation effects, which introduces a strong temperature dependence onto the capture and emission times of the defects. In addition, a popular correction of the SRH model, where an Arrhenius activated capture cross section [10] is introduced, is discussed. It is shown that this modification provides an approximate link between the NMP and SRH models. By investigating defects with larger relaxation energies, which are typically observed in bulk oxide defects, i.e., border traps, the limits of SRH models are demonstrated.

Manuscript received November 27, 2020; revised December 19, 2020; accepted January 3, 2021. Date of publication January 15, 2021; date of current version March 24, 2021. This work was supported by the Austrian Research Promotion Agency (FFG) under Project 881110. This article is an extended version of a paper presented at IEDM 2020. The review of this article was arranged by Editor D. Triyoso. *(Corresponding author: Bernhard Ruch.)*

Bernhard Ruch is with KAI GmbH, 9524 Villach, Austria, and also with the Institute for Microelectronics, TU Wien, 1040 Vienna, Austria (e-mail: bernhard.ruch@k-ai.at).

Markus Jech and Tibor Grasser are with the Institute for Microelectronics, TU Wien, 1040 Vienna, Austria.

Gregor Pobegen is with KAI GmbH, 9524 Villach, Austria.

Color versions of one or more figures in this article are available at https://doi.org/10.1109/TED.2021.3049760.

Digital Object Identifier 10.1109/TED.2021.3049760

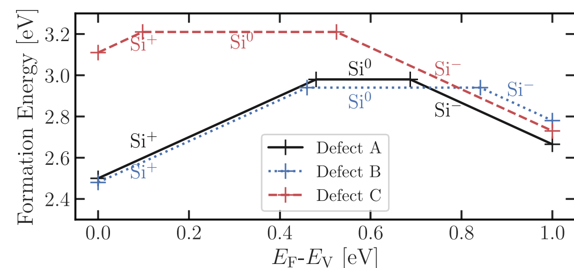

Fig. 1. Formation energies of the defects A–C plotted over the Fermi level with respect to the valance band of Si for the three possible charge states.

II. Microscopic Simulation of Interface Defects

Based on structures created by DFT simulations presented in [6], three promising defect candidates for Si dangling bond (DB) defects, also known as P_b centers, were investigated in greater detail. Those particular Si-DB configurations resemble the well-known geometrical characteristics of a P_b center, a trivalenty bonded Si atom with one unpaired electron in the vicinity of the Si/SiO_2 interface. Furthermore, they possess two charge transition levels, +/0 and 0/−, within the Si bandgap (see Fig. 1)—as expected for P_b centers [7], [8]. The first candidate, defect A, is a Si atom one layer below the interface, trivalently bonded to three other Si atoms missing a fourth bond. Similarly, configuration B features a close-by O atom from the amorphous SiO_2 network. Finally, defect C

This work is licensed under a Creative Commons Attribution 4.0 License. For more information, see https://creativecommons.org/licenses/by/4.0/

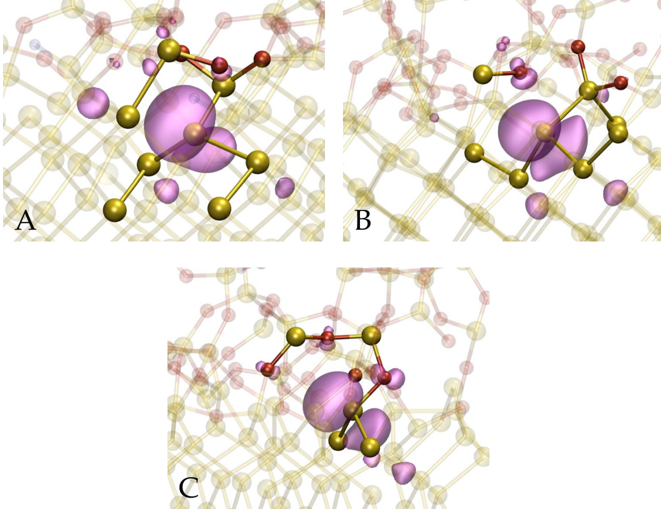

Fig. 2. Spin density of defects A–C. Si atoms are represented in yellow and O atoms in red. Defects A and B miss a forth Si atom in the lattice, while there are no O atoms in the vicinity of A in contrast to B. In defect C, a Si-DB is bonded to one O atom and two Si atoms. Isosurfaces are shown at a value of 0.01 in violet.

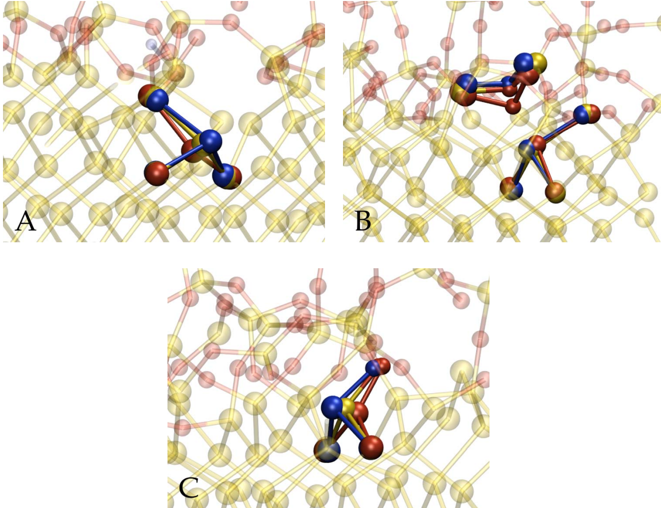

Fig. 3. Structural reconfiguration of defects A–C (left to right) when positively (red), negatively (blue), or neutrally (yellow) charged.

represents a Si-DB that is bonded to one O and two Si atoms. The spin densities clearly show that the unpaired electron is fully localized on the respective defect configuration (shown in Fig. 2). The positively and negatively charged states of the defects are calculated in addition to the neutral state for the chosen configurations [6]. Their structural reconfigurations are shown in Fig. 3. Generally, it is found that the silicon atoms do not significantly change their positions upon charge capture due to the rigid crystalline lattice. However, the a-SiO_2 structure is more flexible and considerable reconfigurations of nearby O atoms can be observed in B and partly C, which is particularly pronounced for the positive charge state.

III. Analytical Trap Models

Point defects in oxides of semiconductor devices are usually separated into interface traps and oxide traps [11]. Interface traps are generally modeled by the SRH model [1], which ignores structural reconfigurations. For defects deeper within an oxide, a more complete approach is always necessary: The NMP model [5], [12] considers spatial changes of the lattice induced by changes in the charge states of defects and can be used for the description of transition rates of charge carriers between the defects and a reservoir. Using the results of the above presented DFT simulations, we chose defect A to extract the parameters for an NMP investigation of interface traps to compare the NMP model, usually used for oxide defects, to the SRH model. The SRH energy barrier [5]

$$\varepsilon_{21}^{\mathrm{SRH}} = -E_{21} \tag{1}$$

for emission transitions is equal to the energy difference between the equilibrium configurations in the two considered charge states (see Fig. 4) and does not consider any additional barriers. In the NMP model, transitions are accompanied by changes in the underlying defect configurations and thereby take an additional relaxation energy

$$\varepsilon_R = \frac{1}{2} M \omega_i^2 \Delta q^2 \tag{2}$$

into account. It can be extracted from the potential energy profiles of the defect states thst are approximated as harmonic potentials (see Fig. 5) [5]

$$V_i = \frac{1}{2} M \omega_i^2 \Delta q^2 + E_i \tag{3}$$

where M is the effective mass of the "defect molecule," ω_i is the vibrational frequency in the minimum i, Δq is the difference between the reaction coordinate and the local equilibrium position, and E_i the potential energy in the minimum. A quadratic fit of the potential for the charged states assuming linear electron-photon coupling ($\omega_i = \omega$ for all i) yields (2) and leads to the activation/transition barrier for emission transitions in the NMP model

$$\varepsilon_{21}^{\mathrm{NMP}} = \frac{(\varepsilon_R - E_{21})^2}{4\varepsilon_R} = \frac{\varepsilon_R}{4} + \frac{E_{21}^2}{4\varepsilon_R} - \frac{E_{21}}{2}. \tag{4}$$

From our DFT simulations, we extract relaxation energies for the charged states. The positively charged state has ε_R of 0.22 eV, and the negatively charged state has ε_R of 0.18 eV. The barrier for capture transitions for both models can be obtained by

$$\varepsilon_{12} = \varepsilon_{21} + E_{21}. \tag{5}$$

In the following, the derivation will focus on both holes and electrons, i.e., electron interactions with the valence band ($E_{21} = E_t - E_V$) and conduction band ($E_{21} = E_C - E_t$). Using the transition barriers for the SRH and NMP model, the hole and electron capture rates are given by

$$k_{12}^{h+} = p v_{\mathrm{th}} \sigma \exp\left(-\frac{\varepsilon_{12}}{k_B T}\right) \tag{6a}$$

$$k_{12}^{e-} = n v_{\mathrm{th}} \sigma \exp\left(-\frac{\varepsilon_{12}}{k_B T}\right) \tag{6b}$$

where p and n are electron and hole concentrations, respectively, σ is the capture cross section, and v_{th} is the thermal carrier velocity. Similarly, the hole and electron emission

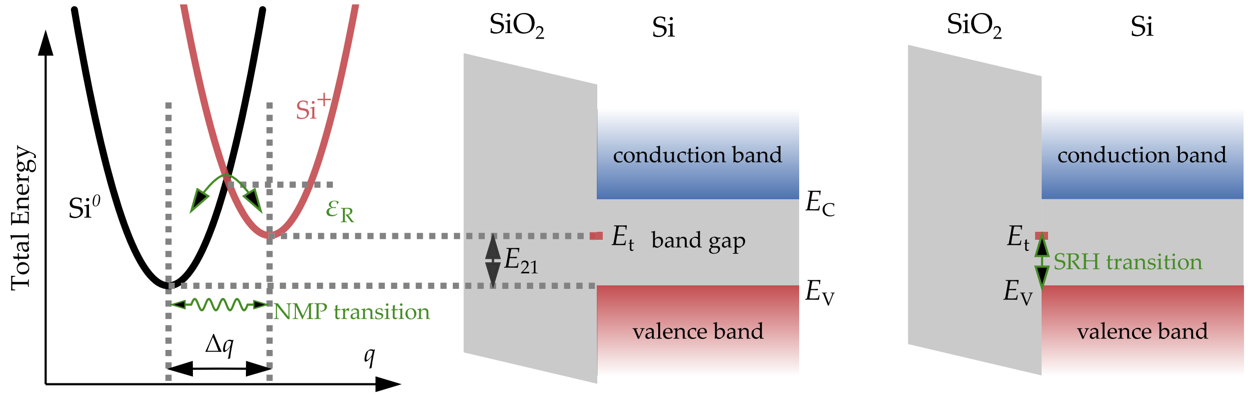

Fig. 4. Schematic comparison of NMP and SRH transitions for holes. NMP transitions consider the barrier between the two states caused by the relaxation energy. Structural relaxation is ignored in the SRH model, and only the electronic energy difference between the trap and valence band energies (E_t and E_V) is considered. Therefore, SRH transitions lack the relaxation energy ε_R barrier present in the NMP model.

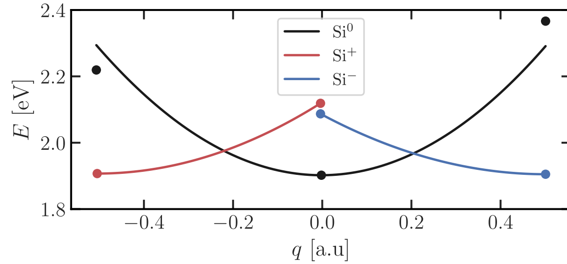

Fig. 5. Potential energy curves of defect A for neutral, positive, and negative charge states along the reaction coordinate q obtained from DFT simulations. A fit with parabolas is used to extract relaxation energies.

transition rates are written as

$$k_{21}^{h+} = N_V v_{\mathrm{th}} \sigma \exp\left(-\frac{\varepsilon_{21}}{k_B T}\right) \quad (7a)$$

$$k_{21}^{e-} = N_C v_{\mathrm{th}} \sigma \exp\left(-\frac{\varepsilon_{21}}{k_B T}\right) \quad (7b)$$

with the numbers of states in valence and conduction band N_V and N_C.

IV. Experimental Structures and Measurement Procedure

We investigated the behavior of interface defects on lateral n-channel MOSFETs with a channel length of 6 μm, a channel width of 100 μm, and a 30-nm SiO_2 insulator. These devices are surrounded by a polycrystalline silicon heater (polyheater), which is used to regulate the device temperature by Joule heating. This is achieved by cooling the structure to a base temperature of −60 °C and applying a precalibrated bias to the polyheater, thereby reaching adjustable temperatures up to approximately 200 °C [13]. All measurements were performed on wafer level, where a temperature-controlled chuck cools the whole wafer to the base temperature. Traps are generated by a 20-ks hot-carrier stress ($V_D = 8$ V and $V_G = 4$ V) at various stress temperatures allowing for a quantitative adjustment of the hot-carrier stress generated traps, as hot-carrier degradation is strongly temperature-dependent [14]. Regular and SPCP [15] were chosen as the main defect characterization method to obtain the density of states of interface traps in the bandgap. Due to the wide temperature range of this measurement method, compared to other charge pumping (CP) methods, the SRH theory can be tested thoroughly as a function of temperature. Generally, the MOS structure under investigation is pulsed from deep inversion to deep accumulation in all CP methods [16]. Defects capturing carriers during the accumulation phase reemit them during the inversion phase and vice versa. This leads to a measurable net current I_{CP} between the n- and p-doped areas near or under the MOS structure, which is in our case between the tied drain and source contacts and the body contact. A parasitic effect of CP, the emission of carriers during the phase in which they are captured, depends on the emission time constants of the traps. Thus, the rise and fall times of the slopes of the applied pulse regulate this parasitic effect. SPCP makes use of this effect by sweeping the rise and fall times of the pulses to energetically scan the bandgap [2]. Later, the rise and fall time sweeps can be transformed into the energetic component of the spectrum, while the change of the CP current is transformed into the density of states. It is noted that the inverse of the transition rates for emission

$$\tau_{\mathrm{em}}^{h+} = \frac{1}{k_{21}^{h+}} = \frac{\left|V_{\mathrm{TH}}^{\mathrm{CP}} - V_{\mathrm{FB}}^{\mathrm{CP}}\right|}{\Delta V_g} t_r \quad (8a)$$

$$\tau_{\mathrm{em}}^{e-} = \frac{1}{k_{21}^{e-}} = \frac{\left|V_{\mathrm{TH}}^{\mathrm{CP}} - V_{\mathrm{FB}}^{\mathrm{CP}}\right|}{\Delta V_g} t_f \quad (8b)$$

is related to the rise and fall times (t_r and t_f) of SPCP. The fraction of the rise and fall times of the CP pulse with an amplitude of ΔV_g that transitions between the threshold voltage and flat-band voltage of CP ($V_{\mathrm{TH}}^{\mathrm{CP}}$ and $V_{\mathrm{FB}}^{\mathrm{CP}}$) is assumed to be equal to the emission time constant τ_{em} [2]. This assumption is based on the idea that emission is only possible when the channel area is neither in inversion nor accumulation. Thus, the energy transformations of the density of states in SPCP for the SRH model are

$$-E_{21}^{\mathrm{SRH}^{h+}} = k_B T \ln\left(\tau_{\mathrm{em}}^{h+} N_V v_{\mathrm{th}} \sigma^{\mathrm{SRH}}\right) \quad (9a)$$

$$-E_{21}^{\mathrm{SRH}^{e-}} = k_B T \ln\left(\tau_{\mathrm{em}}^{e-} N_C v_{\mathrm{th}} \sigma^{\mathrm{SRH}}\right) \quad (9b)$$

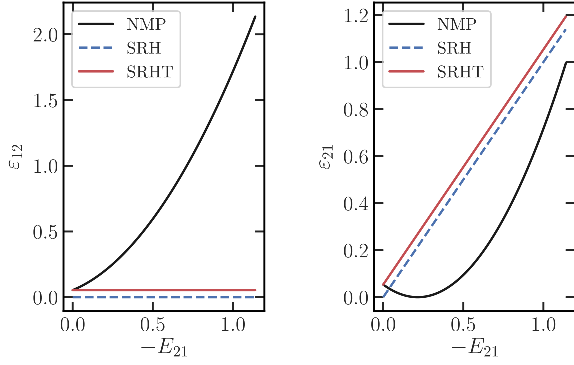

Fig. 6. Approximation (11) of the NMP transition energies compared to the exact calculation. The respective transition energy is also plotted for the SRH model. Left: capture process. Right: emission process.

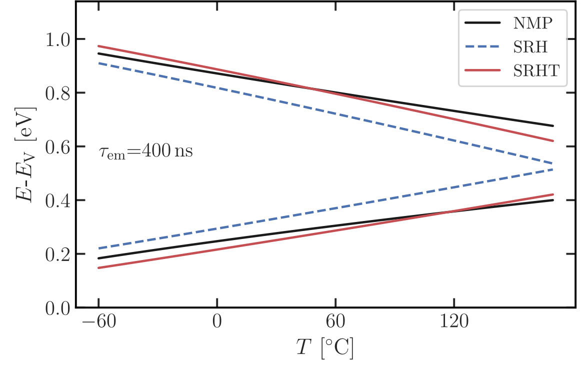

Fig. 7. Temperature dependence of the energetic limits of CP for the NMP, SRH, and SRHT models for a constant value of τ_{em}.

while for the NMP model, the following relations are obtained:

$$-E_{21}^{\text{NMP}^{h+}} = \sqrt{4\varepsilon_R^{h+} k_B T \ln\left(\tau_{\text{em}}^{h+} N_V v_{\text{th}} \sigma^{\text{NMP}}\right)} - \varepsilon_R^{h+} \quad (10a)$$

$$-E_{21}^{\text{NMP}^{e-}} = \sqrt{4\varepsilon_R^{e-} k_B T \ln\left(\tau_{\text{em}}^{e-} N_C v_{\text{th}} \sigma^{\text{NMP}}\right)} - \varepsilon_R^{e-}. \quad (10b)$$

At this point, a connection between the SRH and NMP models can be established assuming energy differences between defects and reservoir which are significantly larger than relaxation energies ($E_{21} \gg \varepsilon_R$). By using a linear approximation

$$\varepsilon_{21}^{\text{NMP}} \approx \varepsilon_R/4 - E_{21} \quad (11)$$

for the relationship of the transition barrier and relaxation energy, the commonly used Arrhenius correction

$$\sigma_{\text{NMP}} \approx \sigma_{\text{SRH}} \exp\left(-\frac{\varepsilon_R}{4k_B T}\right) \quad (12)$$

of capture cross sections [10], [17] can be derived from (7) by comparing the resulting emission rates to the respective SRH rates. The approximation (11), compared to the exact calculation from the NMP model in Fig. 6, differs from the one presented [5] for linear electron-phonon coupling. This is due to the fact that only a linear relationship between E_{21} and $\varepsilon_{21}^{\text{NMP}}$ enables a transformation of capture cross sections by an Arrhenius law. The resulting NMP capture cross section (12) can be used in (9) to obtain the energy transformation of the SRH model with temperature compensation (SRHT)

$$-E_{21}^{\text{SRHT}^{h+}} = k_B T \ln\left(\tau_{\text{em}}^{h+} N_V v_{\text{th}} \sigma^{\text{SRH}}\right) - \frac{\varepsilon_R^{h+}}{4} \quad (13a)$$

$$-E_{21}^{\text{SRHT}^{e-}} = k_B T \ln\left(\tau_{\text{em}}^{e-} N_C v_{\text{th}} \sigma^{\text{SRH}}\right) - \frac{\varepsilon_R^{e-}}{4}. \quad (13b)$$

This adds an offset $-\varepsilon_R/4$ to the SRH energies. The transformation of the CP current to the density of states

$$\frac{dI_{\text{CP}}}{dt_r} = qAf\,D(E_t(t_r))\frac{dE_t}{dt_r} \quad (14a)$$

$$\frac{dI_{\text{CP}}}{dt_f} = qAf\,D(E_t(t_f))\frac{dE_t}{dt_f} \quad (14b)$$

leads to the same spectra for the SRH and SRHT models

$$D^{\text{SRH}}(E_t(t_r)) = \frac{dI_{\text{CP}}}{dt_r}\frac{t_r}{qAf}\frac{1}{k_B T} \quad (15a)$$

$$D^{\text{SRH}}(E_t(t_f)) = \frac{dI_{\text{CP}}}{dt_f}\frac{t_f}{qAf}\frac{1}{k_B T} \quad (15b)$$

known from SPCP literature [2] but a new result for the NMP model, namely

$$D^{\text{NMP}}(E_t(t_r)) = \frac{dI_{CP}}{dt_r}\frac{t_r}{qAf}\sqrt{\frac{\ln\left(\tau_{\text{em}}^{h+} N_V v_{\text{th}} \sigma^{\text{NMP}}\right)}{\varepsilon_R^{h+} k_B T}} \quad (16a)$$

$$D^{\text{NMP}}(E_t(t_f)) = \frac{dI_{CP}}{dt_f}\frac{t_f}{qAf}\sqrt{\frac{\ln\left(\tau_{\text{em}}^{e-} N_C v_{\text{th}} \sigma^{\text{NMP}}\right)}{\varepsilon_R^{e-} k_B T}}. \quad (16b)$$

In the previous equations, q is the elementary charge, A is the interface area investigated by CP, and f is the CP frequency. The CP rise and fall times t_r and t_f in (14)–(16) are transformed from τ_{em}^{h+} and τ_{em}^{e-} according to (8). A complete SPCP spectrum is obtained by sweeping the CP rise and fall times at various temperatures [2].

V. Results and Discussion

Fig. 7 shows the temperature dependence of the trap energies for a given emission time constant for both valence and conduction band interactions. This reflects the maximum possible energy window of CP and SPCP between the respective curves for each model. If we take the more complete NMP model as the benchmark, the SRH model performs worse than the SRHT model, which is not surprising given that the SRHT model considers the relaxation energy in the capture cross section. Given that the energy barrier is approximated in a rather crude manner for the SRHT model (11), it is not surprising that a deviation of this model from the NMP model can be observed. Capture and emission time dependencies of the Fermi level can easily be compared for the three models (NMP, SRH, and SRHT) (see Fig. 8) where the emission rates are constant over the Fermi level as they are independent of the carrier concentration. Neither the SRH nor the SRHT model can perfectly match the NMP model. This imperfection of modeling does not bother us unduly since trap energies of the SRH and SRHT model match well with the NMP model.

A direct comparison of the NMP trap energies to SRH and SRHT trap energies is shown in Fig. 9—for various measurement temperatures. It is found that the SRHT model hardly deviates from the NMP calculations. However, the SRH model, while performing worse, does not significantly deviate either. In order to compare the models to real measurement data, it is necessary to find a suitable capture cross section for the analysis with the three models. Therefore, the trap

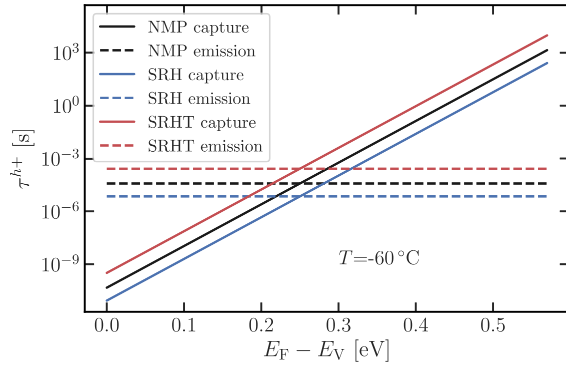

Fig. 8. Comparison of the capture and emission times for NMP, SRH, and SRHT models.

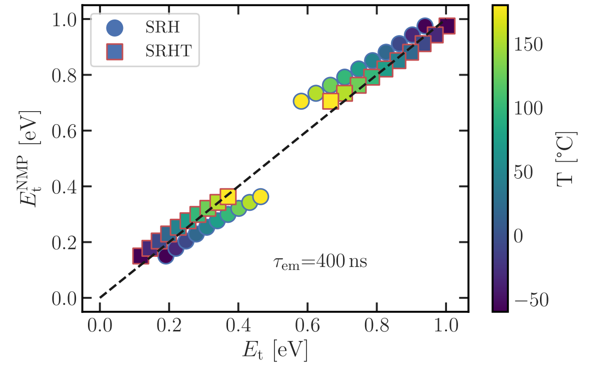

Fig. 9. Comparison of the trap energies in SPCP obtained from the SRH and SRHT models to the trap energies from the NMP model.

density of SPCP N_{spec} obtained from integrating over the $D(E)$ spectrum was compared to the trap density of standard CP N_{std} (see Fig. 10), which is proportional to I_{CP} and thus independent of trap models. The integration of $D(E)$ was performed for varying capture cross sections and four measurements [18]. For improved readability, only one measurement for each model is shown in Fig. 10. From the intersection of the integrated spectra with the standard CP trap value for the respective measurement, the capture cross section can be extracted. This analysis yielded $\sigma_{NMP} = 2.0 \pm 1.3 \times 10^{-16}$ cm^2 for the NMP model, $\sigma_{SRH} = 14 \pm 9.0 \times 10^{-16}$ cm^2 for the SRH model, and $\sigma_{SRHT} = 5.7 \pm 4.3 \times 10^{-16}$ cm^2 for the SRHT model. As predicted by our calculations, the cross sections of the SRH and SRHT models overlapped confirming the validity of assumption (12). The impact of the models on the spectra evaluation of SPCP is presented in Fig. 11 for one measurement. As already observed in earlier analytical calculations, the SRH model again deviates slightly from the NMP model, whereas the SRHT model can predict the energetic positions of the spectrum with respect to the NMP model very well. The SRHT model only corrects the energetic distribution, though, and lacks an adjustment of the values of the density of states due to structural relaxations that are considered in the NMP model.

When integrating the spectra of various measurements at different stress temperatures and comparing the resulting trap densities to standard CP as shown in Fig. 12, taking the variance of the capture cross sections into account, almost no difference in the models can be observed. This indicates that, in this kind of analysis, the deviations of the different models are averaged out by the integration.

However, a closer look at Fig. 6 reveals why the SRH and SRHT models are unsuitable for the modeling of oxide defects though. Higher relaxation energies, which are observed for border traps located deeper in the oxide [19], cause a larger curvature for the parabolic transition energy and, consequently, an even worse fit of the SRH transition energy. The linearized SRHT transition energy (see Fig. 6) is additionally shifted up, thereby drifting even further away from the more complete NMP description. As a consequence, both the SRH model and the SRHT model strongly deviate from the NMP model. This is reflected in the analysis of the SPCP measurement in

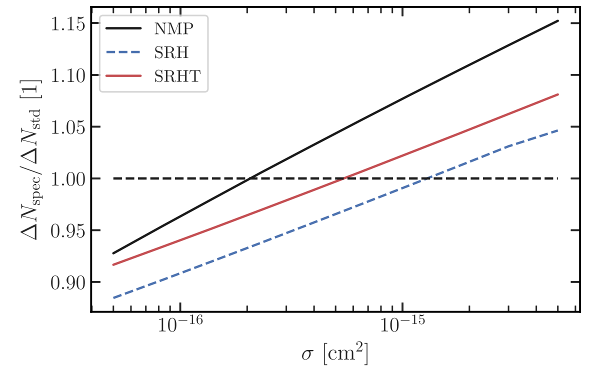

Fig. 10. Extraction method for the capture cross section σ obtained by comparison of integrated $D(E_t)$ spectra and standard CP.

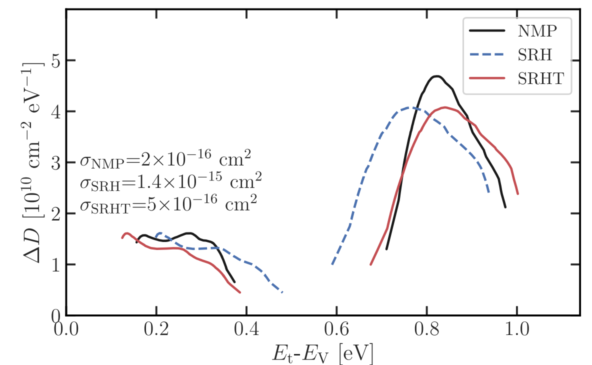

Fig. 11. Comparison of $D(E)$ spectra of SPCP obtained from the NMP, SRH, and SRHT models for a single raw data set of SPCP data. The values of ε_R from our DFT calculations are used.

Fig. 13. It uses the same input data as the evaluation in Fig. 11 but with an increased relaxation energy of 1 eV for both hole and electron transitions. On the one hand, the correction of the magnitude of the density of states due to the relaxation energy is missing. On the other hand, the energetic positions diverge. This is especially pronounced for the SRHT model. This means that an Arrhenius correction of the capture cross section yields incorrect relaxation energies if fit to experimental data.

VI. Conclusion

Charge capture-induced structural relaxations of P_b center candidates, extracted from DFT simulations, are calculated.

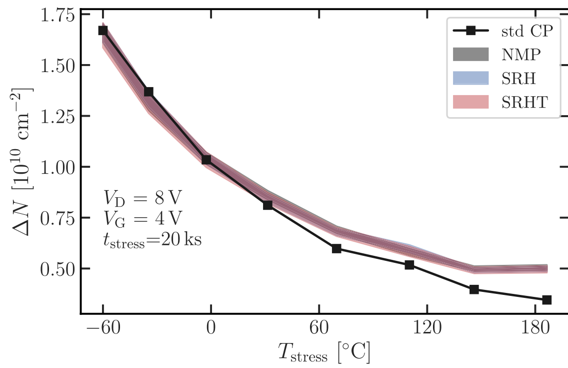

Fig. 12. Comparison of integrated $D(E)$ trap densities and trap densities of standard CP after a hot-carrier stress, where $D(E)$ was obtained from NMP, SRH, and SRHT models. Stress dose varied by changing the temperature during stress.

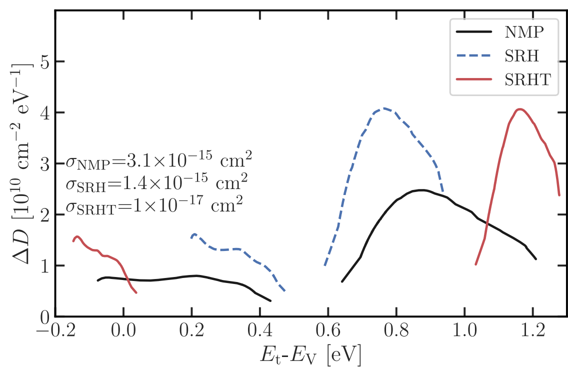

Fig. 13. Comparison of $D(E)$ spectra of SPCP obtained from the NMP, SRH, and SRHT models for a single raw data set of SPCP data. ε_R = 1 eV, representing a hypothetical oxide defect.

These structural relaxations near and at the Si–oxide interface are considered in the NMP model, which is used to benchmark the SRH counterpart against the NMP model. The SRH model does not include this relaxation effect, which, therefore, limits its applicability. The SRH model can be improved by the introduction of an Arrhenius activated capture cross section, which itself can be interpreted as a simplification of the NMP model. All three models are compared for a data set obtained by CP and SPCP. From this comparison, we conclude that the SRH model is an adequately good approximation of the NMP model for the small relaxation energies of interface defects. For these traps, the SRH model can be improved by a temperature-dependent σ. These relatively small structural relaxations, compared to oxide defects, are the main reason that the SRH model could be used for such a long time to describe interface states without major issues. Also, the temperature dependence of defects is often not, or only over a small range, investigated. Thus, temperature-dependent effects can be concealed by an adjustment of the capture cross section, which is a poorly known parameter in any case. At larger relaxation energies, which as those seen for border traps, both the SRH and SRHT models fail. Due to the nature of the SRHT model, which incorporates an Arrhenius activation of the capture cross section, this means that the modification of the capture cross section does not yield correct relaxation energies when fitted to experimental data. In any case, the SRHT model should only be regarded as a case study, which demonstrates the transition from the NMP model to the SRH model using Arrhenius activated capture cross sections. Since relaxation energies are required for both the NMP and SRHT models, the NMP model should always be preferred for the evaluation of transition rates.

References

[1] W. Shockley and W. T. Read, “Statistics of the recombinations of holes and electrons,” *Phys. Rev.*, vol. 87, no. 5, pp. 835–842, Sep. 1952.

[2] T. Aichinger and M. Nelhiebel, “Advanced energetic and lateral sensitive charge pumping profiling methods for MOSFET device characterization—Analytical discussion and case studies,” *IEEE Trans. Device Mater. Rel.*, vol. 8, no. 3, pp. 509–518, Sep. 2008.

[3] T. Tsuchiya, “Interactions between interface traps in electron capture/emission processes: Deviation from charge pumping current based on the Shockley–Read–Hall theory,” *Appl. Phys. Exp.*, vol. 4, no. 9, 2011, Art. no. 094104.

[4] P. Masson, J.-L. Autran, M. Houssa, X. Garros, and C. Leroux, “Frequency characterization and modeling of interface traps in $HfSi_xO_y/HfO_2$ gate dielectric stack from a capacitance point-of-view,” *Appl. Phys. Lett.*, vol. 81, no. 18, pp. 3392–3394, 2002.

[5] T. Grasser, “Stochastic charge trapping in oxides: From random telegraph noise to bias temperature instabilities,” *Microelectron. Rel.*, vol. 52, no. 1, pp. 39–70, Jan. 2012.

[6] M. Jech, A.-M. El-Sayed, S. Tyaginov, A. L. Shluger, and T. Grasser, “*Ab initio* treatment of silicon-hydrogen bond rupture at Si/SiO_2 interfaces,” *Phys. Rev. B, Condens. Matter*, vol. 100, Nov. 2019, Art. no. 195302.

[7] A. Stesmans, “Structural relaxation of P_b defects at the (111)Si/SiO_2 interface as a function of oxidation temperature: The P_b-generation–stress relationship,” *Phys. Rev. B, Condens. Matter*, vol. 48, pp. 2418–2435, Jul. 1993.

[8] L.-A. Ragnarsson and P. Lundgren, “Electrical characterization of P_b centers in (100)Si–SiO_2 structures: The influence of surface potential on passivation during post metallization anneal,” *J. Appl. Phys.*, vol. 88, no. 2, pp. 938–942, 2000.

[9] Y. Nishi, “Study of silicon-silicon dioxide structure by electron spin resonance I,” *Jpn. J. Appl. Phys.*, vol. 10, no. 1, pp. 52–62, Jan. 1971.

[10] M. J. Kirton and M. J. Uren, “Capture and emission kinetics of individual Si:SiO_2 interface states,” *Appl. Phys. Lett.*, vol. 48, no. 19, pp. 1270–1272, 1986.

[11] D. M. Fleetwood, “‘Border traps’ in MOS devices,” *IEEE Trans. Nucl. Sci.*, vol. 39, no. 2, pp. 269–271, Apr. 1992.

[12] B. K. Ridley, *Quantum Processes Semiconductors*. Oxford, U.K.: Oxford Univ. Press, 2013.

[13] G. Pobegen, M. Nelhiebel, S. de Filippis, and T. Grasser, “Accurate high temperature measurements using local polysilicon heater structures,” *IEEE Trans. Device Mater. Rel.*, vol. 14, no. 1, pp. 169–176, Mar. 2014.

[14] F.-C. Hsu and K.-Y. Chiu, “Temperature dependence of hot-electron-induced degradation in MOSFET’s,” *IEEE Electron Device Lett.*, vol. 5, no. 5, pp. 148–150, May 1984.

[15] G. Van Den Bosch, G. V. Groeseneken, P. Heremans, and H. E. Maes, “Spectroscopic charge pumping: A new procedure for measuring interface trap distributions on MOS transistors,” *IEEE Trans. Electron Devices*, vol. 38, no. 8, pp. 1820–1831, Aug. 1991.

[16] G. Groeseneken, H. E. Maes, N. Beltran, and R. F. De Keersmaecker, “A reliable approach to charge-pumping measurements in MOS transistors,” *IEEE Trans. Electron Devices*, vol. 31, no. 1, pp. 42–53, Jan. 1984.

[17] C. H. Henry and D. V. Lang, “Nonradiative capture and recombination by multiphonon emission in GaAs and GaP,” *Phys. Rev. B*, vol. 15, no. 2, pp. 989–1016, Jan. 1977.

[18] B. Ruch, G. Pobegen, and T. Grasser, “Investigation of the temperature dependence of hot-carrier degradation in Si MOSFETs using spectroscopic charge pumping,” *IEEE Trans. Electron Devices*, vol. 67, no. 10, pp. 4092–4098, Oct. 2020.

[19] W. Goes *et al.*, “Identification of oxide defects in semiconductor devices: A systematic approach linking DFT to rate equations and experimental evidence,” *Microelectron. Rel.*, vol. 87, pp. 286–320, Aug. 2018.